Resonantly enhanced multiphoton ionization and zero kinetic energy photoelectron spectroscopy of Benzo[*e*]pyrene

Colin Harthcock, Jie Zhang, and Wei Kong*

Department of Chemistry, Oregon State University,

Corvallis, Oregon 97331-4003

Manuscript for submission to the journal of *Chemical Physics Letters*, September 13, 2012

* Corresponding author, wei.kong@oregonstate.edu, 541-737-6714.

Abstract:

We report zero kinetic energy (ZEKE) photoelectron spectroscopy via resonantly enhanced multiphoton ionization (REMPI) for benzo[*e*]pyrene. Extensive vibronic coupling between the first electronically excited state and a nearby state allows b_2 symmetric modes to be observed which would normally be Franck-Condon (FC) disallowed. These vibronic modes are comparable in intensity to the FC allowed a_1 modes. Gaussian 09 is able to qualitatively simulate the vibronic spectra of the REMPI and the ZEKE experiment using density functional methods. The ZEKE spectra demonstrate propensity in preserving the vibrational excitation of the intermediate electronic state. These results suggest a remarkable structural stability of B*e*P in accommodating the additional charge.

Key words:

photoionization spectroscopy, polycyclic aromatic hydrocarbons, zero kinetic energy photoelectron spectroscopy, far infrared vibrational spectroscopy, vibronic coupling.

Introduction

Polycyclic aromatic hydrocarbons (PAHs) are a group of molecules that are observed in pollution, in comet tails, and possibly in the interstellar medium. In biology, PAHs are lipophilic and many are known carcinogens.[1-3] In astrobiology, it has been hypothesized that PAHs could be related to the origin of life by forming the first primitive organic molecules including amino acids in the pre-DNA world.[4-6] In astrophysics, PAHs have been observed in a wide range of galactic and extragalactic environments.[7-8] They are considered responsible for a range of spectroscopic absorption and emission features, and hence their rovibronic quantum states have substantial implications to the energy balance in the universe.[9-16]

Many spectroscopic studies of neutral and cationic PAHs have been motivated by astrophysical modeling.[17-24] Both the infrared and visible/ultraviolet regions have been extensively investigated using photoionization spectroscopy, cavity ringdown, as well as infrared absorption and emission spectroscopy techniques.[18, 25-29] The far-infrared (FIR) region has been largely untouched because of issues related to the detector sensitivity and light source intensity. On the other hand, the FIR region is occupied by skeletal vibrations of the molecular frame, and it is considered the "finger-print region" for spectroscopic identification of astrophysical PAHs.

The technique of zero kinetic energy (ZEKE) photoelectron spectroscopy offers an indirect solution to the challenges in the FIR for laboratory astrophysics.[30] In recent years, we have undertaken the mission of mapping out the low frequency vibrational modes of PAHs using ZEKE spectroscopy.[31-36] So far we have reported 3 peri-condensed species including pyrene, benzo[*a*]pyrene (B*a*P), benzo[*g,h,i*]perylene (B*ghi*P), and 3 cata-condensed species including tetracene, pentacene, and chrysene.[31-36] In this report, we investigate the vibronic spectra of

benzo[*e*]pyrene, an isomer of B*a*P as shown in the inset of Figure 1. While the highly carcinogenic isomer B*a*P has been extensively investigated previously,[36-41] B*e*P has only been reported in a few studies.[21, 42-43] We use resonantly enhanced multiphoton ionization (REMPI) to probe the vibronic structure of the first excited electronic state S_1, and the ZEKE technique to probe the skeletal modes of the cationic state D_0. Additional insights can be obtained from comparisons with other PAHs and theoretical calculations.

Experimental setup

The experimental apparatus is a differentially pumped molecular beam machine, with the detection chamber enclosed inside the source chamber.[32, 44] A time-of-flight mass spectrometer in the detection chamber also serves as the pulsed field ionization zero kinetic energy photoelectron spectrometer. The sample benzo[*e*]perylene (Aldrich) was housed and heated to 260 ºC in the pulsed valve located in the source chamber to achieve sufficient vapor pressure. The vapor was seeded in 400 torr of argon and co-expanded into vacuum through a pulsed valve with a 1 mm orifice. After passing through a 2 mm skimmer, the cooled sample reached the detection chamber for laser excitation and ionization. The laser systems for the REMPI experiment included two Nd:YAG (Spectra Physics, GCR 190 and GCR 230) pumped dye lasers (Laser Analytical System, LDL 20505 and LDL 2051), both equipped with frequency doublers. The excitation laser in the 370 - 350 nm range had a typical pulse energy of > 1.0 mJ/pulse with a bandwidth of 0.5 cm^{-1}. The ionization laser in the 300 - 309 nm range had a pulse energy of ~1 mJ/pulse with a bandwidth of 0.3 cm^{-1}. The absolute wavelength of each laser was calibrated using an iron hollow-cathode lamp filled with neon. The pump laser and ionization laser were set to counter-propagate, and the light path, the flight tube, and the

molecular beam were mutually perpendicular. Two delay generators (Stanford Research, DG 535) controlled the timing of the lasers, and the optimal signal was obtained under temporal overlap between the pump and ionization lasers. In the ZEKE experiment, molecules were excited to high Rydberg states for 600 ns in the presence of a small constant DC spoiling field, after which ionization and extraction were achieved by a pulsed electric field of ~2 V/cm.

The Gaussian 09 suite [45]was used to optimize the molecular structure, to obtain vibrational frequencies, and to simulate the observed vibronic structures from REMPI and ZEKE.[45] For the ground state of the neutral and the cationic state, density functional theory (DFT) calculations using the B3LYP functional were performed with the 6-311G basis set. The excited state S_1 was calculated using both time dependent density functional theory (TD-DFT) with the B3LYP functional and the 6-311G basis set and the configuration interaction singles (CIS) with the 6-31G basis set. Details of the calculations will be provided in the following.

Results

Two-color 1+1' REMPI spectroscopy

The 1+1' REMPI spectrum was collected near the origin of the $S_1 \leftarrow S_0$ electronic transition of B*e*P and is displayed in Figure 1. The ionization laser was set at 33,000 cm^{-1} and was temporally and spatially overlapped with the scanning resonant laser. The origin was observed to be 26,983 ± 5 cm^{-1}, which is 9 cm^{-1} higher than the origin reported by Misawa *et. al.* (no uncertainty was reported in this reference).[43] The other observed vibronic transitions are listed in Table I, with the labeling scheme following the Herzberg convention. For clarity, the molecular axes have been included in an inset of the figure.

Based on our previous experience, PAHs are prone to vibronic coupling.[32-36, 44]

Fortunately, Gaussian 09 incorporates a new feature of Herzberg-Teller (HT) coupling, which in general, yields outstanding accuracy in transition frequencies and vibrational intensity distribution. Figure 2 shows the comparison of calculation results with the experimental spectrum. Given the possibility of order switching in the calculated electronic states,[33-36, 46-48] we performed two calculations, one to the putative S_1 (A_1) state with the keyword root = 1 and the other to the putative S_2 (B_2) state with root = 2. Both were at the B3LYP/6-311G level for the excited electronic state. In Fig. 2, the transition to the S_1 (A_1) state is clearly a better match to the experimental spectrum, with a diminished origin band and an intense cluster of bands at ~ 750 cm^{-1}. The calculation for the S_1 (A_1) ← S_0 (A_1) transition also states that the oscillator strength derives from the near degenerate pairs of LUMO ← HOMO-1 and LUMO+1 ← HOMO, where HOMO and LUMO represent the highest occupied molecular orbital and the lowest unoccupied molecular orbital respectively. The transition to the S_2 state, on the other hand, is of LUMO ← HOMO in nature.

While the agreement between calculation and experiment is not quantitative, it is good enough for a general guidance regarding vibrational assignment. In Table I and Fig. 1, most bands are assigned as a_1 or b_2 modes of the C_{2V} point group, and the presence of the latter modes is a pure result of vibronic coupling with the nearby S_2 (B_2) state. The current assignment further results in a scaling factor of 0.973 for the theoretical frequencies. Overall the spectrum has a weak origin band, and the relative intensities of the Franck-Condon (FC) allowed a_1 bands and the FC forbidden but vibronic allowed HT bands are similar.

Assignment of the vibronic structure is straightforward for the first few low frequency modes, but high energy bands are problematic. The cluster of peaks at 750 cm^{-1} is challenging to assign for several reasons. The theoretical calculation could only reproduce the first two peaks of

the triplet feature (inset of Fig. 2c), which can be assigned as mode 84 ($7b_2$) and 26 ($6a_1$). In Table I, the second harmonic of mode $2a_1$ and the fundamental frequency of $6a_1$ are essentially degenerate, and both are higher than the $7b_2$ band by ~5 cm^{-1}. We believe that the high intensity of the $2a_1^2$ band is related to the complication of this Fermi resonance among all three bands. The band at 917 cm^{-1} could be assigned as a combination of $2a_1$ and $4a_1$, but based on the calculation, it probably belongs to a $8b_2$ band, which has a larger deviation (12 cm^{-1}) than the combination band (7 cm^{-1}). A few other bands, such as those at 1282, 1378, and 1571 cm^{-1}, can also be assigned as combination bands or fundamental bands of higher frequency modes. Unlike the $8b_2$ bands, however, these bands are not reproduced from the simulation spectrum and hence the only criterion for their assignment comes from the theoretical frequencies. The listed assignment in Table I is therefore tentative for these bands.

All observed modes are in-plane deformation modes. Similar to our previous observation on B*a*P,[36] the modes of B*e*P can be categorized into three groups, including two groups localized in the pyrene (modes 30, 89, and 28) and the benzene (modes 90) moieties, and the overall skeletal deformation of the molecular frame (modes 84, and 26).[31, 36] The lowest frequency mode 90 is essentially wagging of the benzene ring around the short axis of the pyrene backbone. The next three low frequency modes are in-plane deformations or wagging of the pyrene moiety, with the additional benzene ring tagging along and making no observable internal structural changes. It is interesting to note that while B*a*P and B*e*P belong to very different point groups, they both seem to surrender to the extreme stability of the pyrene moiety in exhibiting localized vibrational modes on pyrene or the additional benzene ring.[36, 44]

ZEKE Spectroscopy

By setting the first laser at one of the intermediate states identified in the above experiment and scanning the second laser, we were able to observe the vibrational bands of the D_0 electronic state using pulsed field ionization ZEKE. Figures 3 and 4 show the ZEKE spectra collected from the eight intermediate states labeled in Fig. 1 in bold-phased fonts. Unfortunately, efforts of recording more ZEKE spectra for intermediate levels with more than 800 cm^{-1} vibrational energies were unsuccessful, particularly for the $16a_1$ band at 1312 cm^{-1}, which is the strongest band in the REMPI spectrum. The spectral assignment, together with the calculation results scaled by 0.9697, is listed in Table II. The spectrum from the origin band of Fig. 1a corresponds to the origin of the cation, which results in an adiabatic ionization threshold of 59,766 ± 7 cm^{-1}, including corrections due to the pulsed electric field. This value is about 100 cm^{-1} below what reported by Clar and Schmidt based on photoelectron spectroscopy (7.41 eV).[49]

The most striking feature of Figure 3 is the lack of any vibrational structure beyond the single transition corresponding to the same vibrational mode (termed diagonal bands in the following) of the intermediate state. This simplicity in the ZEKE spectra is an exemplary case of propensity reported in our studies of substituted aromatic compounds and a few PAHs.[32-36, 44, 50-51] The dominance of the diagonal band manifests the diagonal Franck-Condon factor between the intermediate state and the cationic state. This means that the geometry and normal modes of B*e*P do not change upon ionization. Based on this belief, assignment of the ZEKE spectra in Figure 4 relies on the correlation with the mode of the resonant state. For example, similar to the REMPI spectrum, the cluster of vibrational bands near 750 cm^{-1} is again congested with many closely spaced transitions. In Table II, although the $7b_2$ and $2a_1^2$ bands are degenerate from calculation, the transition in Fig. 4d at 759 cm^{-1} is assigned $2a_1^2$ because of the identity of the intermediate vibronic state.

Simulation of the ZEKE transition from the origin of the intermediate state is shown in the inset of Fig. 3a. The simulated ZEKE spectrum has an intense origin, with essentially no other observed transitions on the scale of the inset. Although vibronic coupling plays an important role in the REMPI process, the next step of ionization strictly follows the Franck-Condon principle. Moreover, there is minimal structural change upon elimination of the excited electron from S_1.

Discussions

Vibrational band distributions and implications in geometry variation

The REMPI spectrum contains both Franck-Condon allowed a_1 bands and vibronic allowed b_2 bands, and overall the two types of bands are of comparable intensity. In addition, the origin band is considerably weaker than a few of the vibronic bands. While the former observation implies extensive vibronic coupling, the latter seems to imply large geometry changes upon electronic excitation. Upon ionization, the ZEKE spectra contain almost exclusively diagonal bands, alluding to an invariant molecular frame with the removal of the electron from the intermediate state. In addition, the vibrational frequencies of the corresponding modes of the S_1 and D_0 states are similar. Although one electron is missing between the two states, the bond strengths, at least for those related to the skeletal motions below 1500 cm^{-1}, remain largely unchanged.

Our calculated molecular structures, on the other hand, paint a picture of stability of B*e*P for all three related electronic states. The overall length and width of the molecular structure vary less than 1% in all cases, similar to the degree of variation for tetracene and pentacene, and slightly larger than the other peri-condensed systems we have reported (~0.5%).[32-34, 36, 44]

The weak origin band thus seems to be not related to large geometry changes.

The extensive vibronic coupling in the REMPI spectrum of B*e*P is confirmed from the Franck-Condon calculation without the HT option in Fig. 2b. The resulting origin band becomes so strong that it dominates the REMPI spectrum. Among all the peri-condensed PAHs we have investigated,[34, 36, 44] the degree of vibronic coupling in B*e*P is by far the most extensive. For cata-condensed species, an even more extreme case was observed in pentacene.[32-33, 35] While our Gaussian calculation with and without HT both predicted overwhelmingly strong totally symmetric a_1 modes for the REMPI spectrum of pentacene, the experimental spectrum contained only FC forbidden out-of-plane waving modes. On the other hand, the electronic transition in pentacene was fully symmetry allowed, and the S_2 state was over 5000 cm^{-1} higher in energy than the S_1 state. The energy gaps between the two lowest excited electronic states vary from 2000 cm^{-1} to over 5000 cm^{-1} among B*e*p, B*a*p, B*ghi*p, pyrene, tetracene, chrysene, and pyrene, and these values do not seem to have a direct correlation with the degree of HT coupling.[32-36, 44] Currently, we do not have an explanation for the seemingly extraordinary degree of vibronic coupling in B*e*P and in pentacene.

All observed modes are in plane deformation modes, and all are IR active for this C_{2V} system. The vibrational levels of the neutral ground state S_0 and the cationic state D_0 of B*e*P have been probed by gas chromatography/Fourier transform infrared spectroscopy (GC/FT-IR) and matrix isolation spectroscopy (MIS) in the region above 600 cm^{-1}.[17, 21] Neither groups performed high level *ab initio* or density functional calculations, hence the vibrational assignment was based on comparisons with other PAHs. For the S_0 state, several bands between 700 and 900 cm^{-1} were considered out-of-plane C-H bending modes, and one band at ~700 cm^{-1} was assigned as C-C in-plane bending. The corresponding modes of the D_0 state were compared

with those of the S_0 states, and the result was regarded as unusual by the authors.[17] While the C-C in-plane mode was *red* shifted by 62 cm^{-1}, the C-H out-of-plane modes were *blue* shifted by nearly ~80 cm^{-1}. Furthermore, the intensities of these bands were also an order of magnitude too low compared with those of their neutral counterparts. Within the region of spectral overlap, unfortunately, we did not observe any common modes with the previous studies, hence no direct frequency comparisons are possible. We do notice interestingly that the general spectral intensity distribution of the GC/FT-IR spectrum is somewhat similar to our REMPI spectrum of Fig. 1, with intense activities between 700 and 900 cm^{-1}. Since the two techniques probe two different electronic states and follow completely different selection rules, this similarity should be a mere coincidence. Nevertheless, bands in this region seem to be particularly sensitive to any changes in the internal energy of the molecular system, as observed in our other studies of PAHs.[32-36, 44] As to the unusual vibrational frequency shifts in the D_0 state,[17] the similarity in frequency between the neutral and the cationic state of our gas phase experiment implies nothing extraordinary in the force field and molecular structure of B*e*P. Most likely, these shifts were due to the influence of the argon matrix in the MIS experiment.

The geometry, Mulliken charge distribution and IR spectroscopy have all been calculated in a separate work by Pathak and Rastogi for both the neutral and cation using B3LYP/4-31G.[52] The reported geometries and charge distributions can be related to our results by a scaling factor, arising from the difference in the two basis sets.

Comparisons with other PAHs

Most of the peri-condensed PAHs that we have investigated so far, including B*a*P, B*e*P, and B*ghi*P, have been reasonably successful for vibrational assignment and spectral simulation,

particularly with the vibronic coupling feature of Gaussian 09.[34, 36, 45] All peri-condensed PAHs and chrysene have at least two closely spaced excited electronic states. In many cases, CIS calculations from Gaussian suffer from the confusion of the closely spaced states, and a keyword has to be set artificially to avoid the problem.[44, 46-48] Even with this confusion, on the other hand, HT calculations based on the displacement vectors and frequencies are still satisfactory in reproducing the observed REMPI spectrum, and with the use of scaling factors, the observed vibrational bands for both S_1 and D_0 can be assigned.

This situation is somewhat different for the cata-condensed species including tetracene, pentacene, and chrysene.[32-33, 35] While tetracene is an example of mostly Franck-Condon behavior for REMPI, chrysene, an isomer with just a kink in the ribbon structure, could not be reproduced satisfactorily in vibronic transition intensities.[32, 35] With an additional ring than tetracene, pentacene is an extreme with no Franck-Condon allowed vibrational bands observable in the REMPI spectrum and no calculation methods were able to even qualitatively reproduce the vibronic features.[32-33] However, the vibrational frequencies for cationic tetracene and pentacene obtained from DFT calculations are so close to the experimental values that no scaling factors are necessary. Moreover, neither molecule has closely spaced excited electronic states for vibronic coupling.

Although seemingly simple, the above comparison alludes to the fact that each PAH has its unique situation, and a generalization of properties is questionable at this stage. Overall, the HT feature in Gaussian 09 has dramatically improved our abilities in modeling the REMPI and ZEKE spectroscopy of peri-condensed species. However, human interference is still necessary for the choice of the correct electronic state and for vibrational scaling. The cata-condensed systems are still difficult to model for *ab initio* or DFT calculations.

An interesting observation in the ZEKE experiment of the PAHs is the existence of a cutoff energy of the intermediate state: when the excess vibrational energy of the intermediate state is above a certain value, for example, 800 cm^{-1} for B*e*P, no more ZEKE signal can be observed from the intermediate state. In chrysene, we also observed mode selectivity in the overall ZEKE signal.[35] The cutoff energy does not seem to have a direct correlation with the size of the molecular system; for the largest molecule B*ghi*P among our studies, we were able to record ZEKE spectrum from bands with nearly 1100 cm^{-1} vibrational energy.[34]

Conclusion

The vibrational spectra of benzo[*e*]pyrene were recorded for both the first electronically excited state and the ground state of the cation. Vibronic coupling was observed to play a major role in the REMPI spectrum, and the intensities of FC forbidden but vibronic allowed bands are similar to those of FC allowed bands. Using the relatively new feature of Gaussian 09, we were able to include Herzberg-Teller coupling for the simulation of the REMPI spectrum with satisfactory results. The ZEKE spectra demonstrate a propensity for preserving the vibrational excitation of the intermediate state, but as the energy excess from the origin of the S_1 state increases to ~800 cm^{-1}, no more ZEKE signal was observable, similar to our previous report on B*ghi*P and chrysene. All observed modes are IR active, but a direct comparison with results from matrix isolation spectroscopy is impossible due to lack of common vibrational modes. Nevertheless, the small variation of vibrational frequency from S_1 to D_0 of our experiment does reveal some unsettling effect of the argon matrix in shifting the frequency and changing the transition intensity.

Acknowledgement

This work is supported by the National Aeronautics and Space Administration under award No. NNX09AC03G.

Figure captions

Figure 1. REMPI spectrum of benzo[*e*]pyrene. The spectrum is shifted by 26,983 cm^{-1} -- the origin of the $S_1 \leftarrow S_0$ transition -- to emphasize the frequencies of the different vibrational modes of the S_1 state. The molecular structure and the definition of molecular axes are also shown in the inset.

Figure 2. Comparison between different calculations of the vibronic spectra using Gaussian 09 for both the $S_1 \leftarrow S_0$ (b & c) and the $S_2 \leftarrow S_0$ transitions (a) with the experiment (d). The calculation without Herzberg-Teller coupling for the $S_1 \leftarrow S_0$ transition (b) is also shown for comparison. An inset is included in the calculation with HT coupling (c) to show the detail in the 730-765 cm^{-1} region.

Figure 3. Two-color ZEKE spectra of B*e*P recorded via the following vibrational levels of the S_1 state as intermediate states: (a) 0^0, (b) 90^1, (c) 30^1, and (d) 89^1. The energy in the figure is relative to the ionization threshold at 59,766 cm^{-1}. The assignment in the figure refers to the vibrational levels of the cation, and the corresponding vibrational level of the intermediate state is labeled by a black dot in each panel. An inset is included in (a) to show the Franck-Condon result from the origin band of S_1.

Figure 4. Two-color ZEKE spectra of B*e*P recorded via the following vibrational levels of the S_1 state as intermediate states: (a) 28^1, (b) 84^1, (c) 26^1, and (d) 30^2. The energy in the figure is relative to the ionization threshold at 59,766 cm^{-1}. The assignment in the figure refers to the vibrational levels of the cation, and the corresponding vibrational level of the intermediate state is labeled by a black dot in each panel.

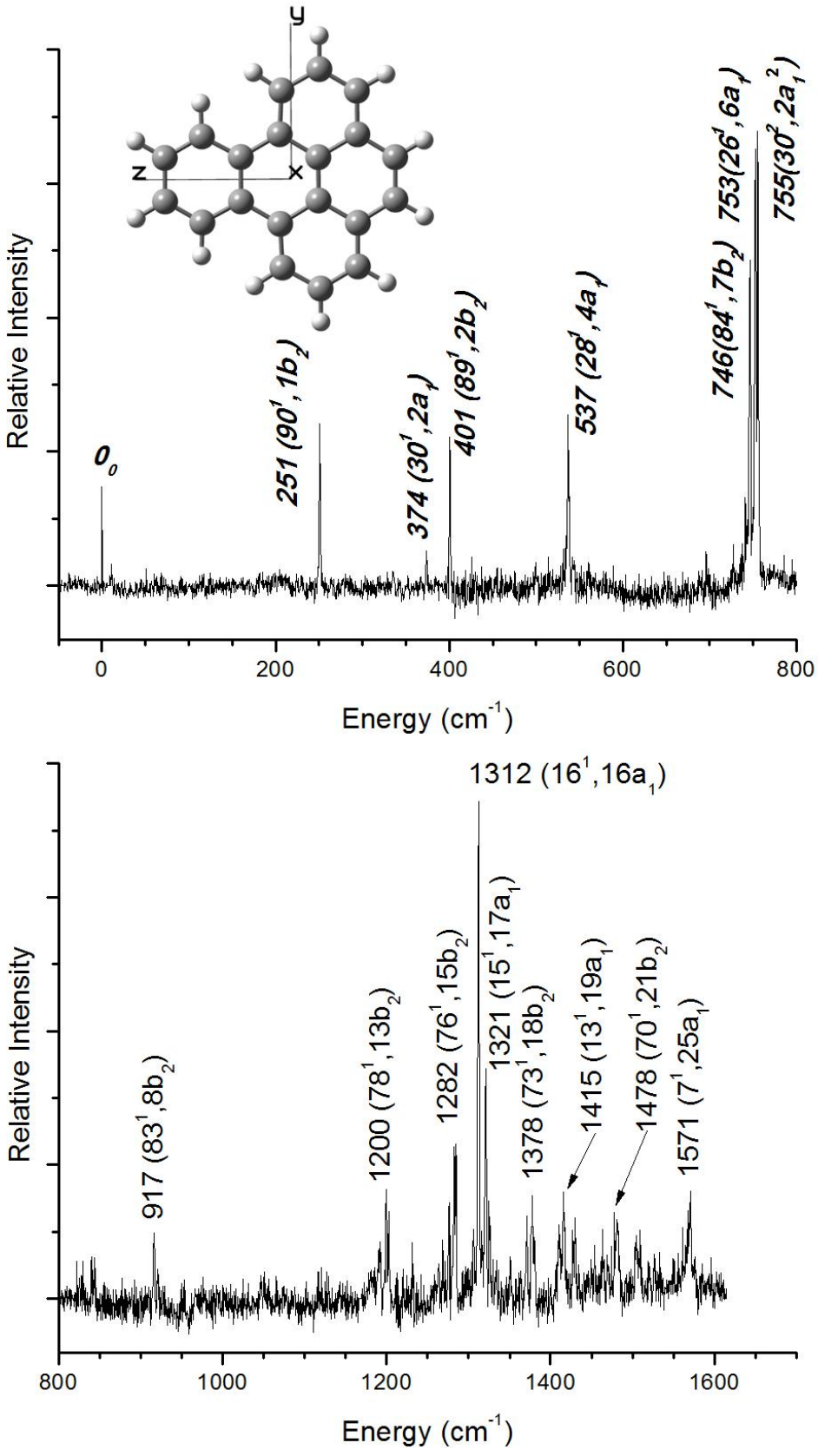
Relative Intensity
Energy (cm-1)
0
200
400
600
800
0₀
251 (90¹,1b₂)
374 (30¹,2a₁)
401 (89¹,2b₂)
537 (28¹,4a₁)
746(84¹,7b₂)
753(26¹,6a₁)
755(30²,2a₁²)
N
C
Relative Intensity
Energy (cm-1)
800
1000
1200
1400
1600
917 (83¹,8b₂)
1200 (78¹,13b₂)
1282 (76¹,15b₂)
1312 (16¹,16a₁)
1321 (15¹,17a₁)
1378 (73¹,18b₂)
1415 (13¹,19a₁)
1478 (70¹,21b₂)
1571 (7¹,25a₁)

Fig. 1

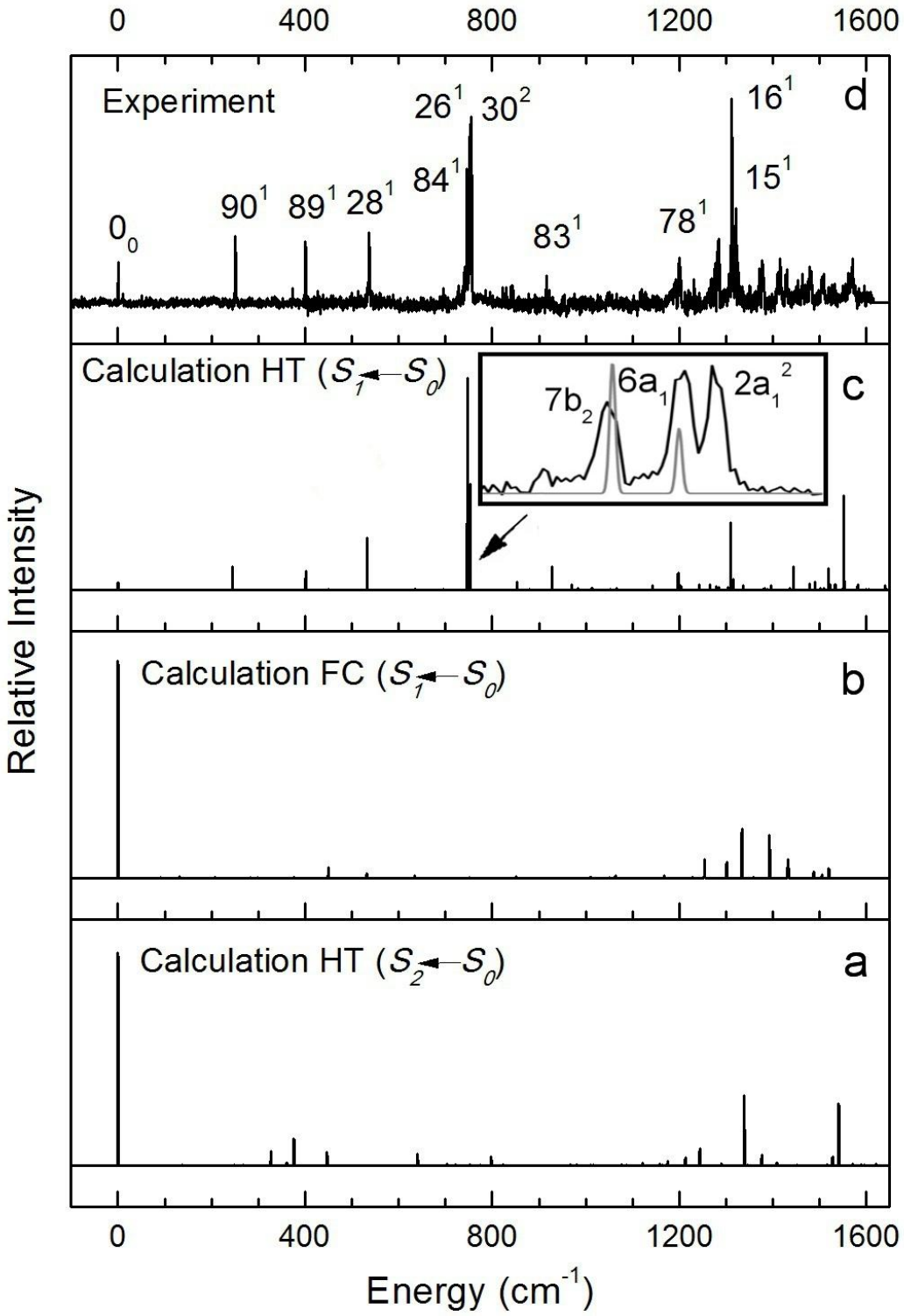
0
400
800
1200
1600
Experiment
26^1
30^2
16^1
d
84^1
15^1
90^1
89^1
28^1
0_0
83^1
78^1
Calculation HT ($S_1 \leftarrow S_0$)
$7b_2$
$6a_1$
$2a_1^2$
c
Calculation FC ($S_1 \leftarrow S_0$)
b
Calculation HT ($S_2 \leftarrow S_0$)
a
Relative Intensity
Energy (cm^{-1})

Fig. 2

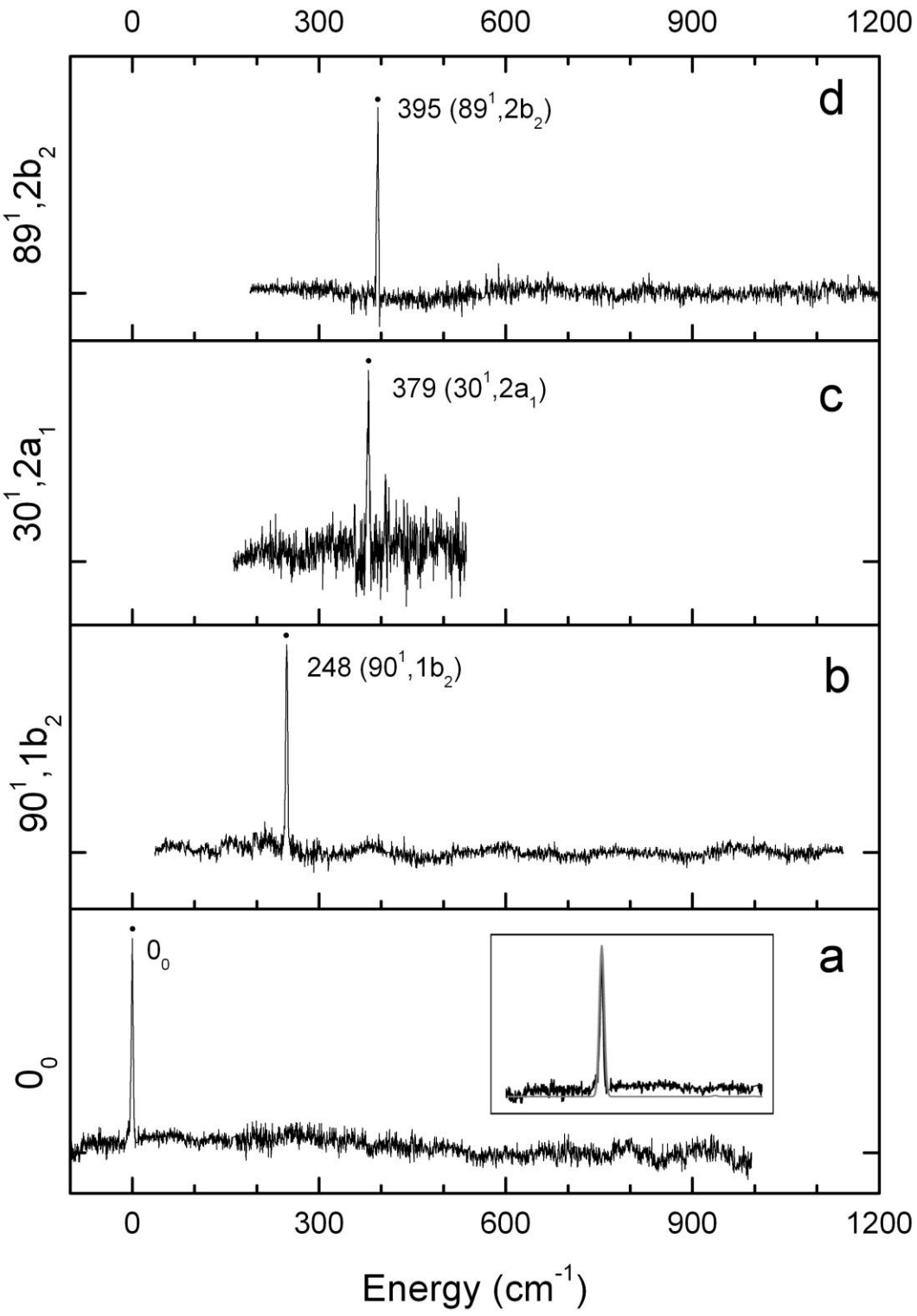
0
300
600
900
1200
d
395 (89^1,2b$_2$)
89^1,2b$_2$
c
379 (30^1,2a$_1$)
30^1,2a$_1$
b
248 (90^1,1b$_2$)
90^1,1b$_2$
a
0$_0$
0$_0$
0
300
600
900
1200
Energy (cm^{-1})

Fig. 3

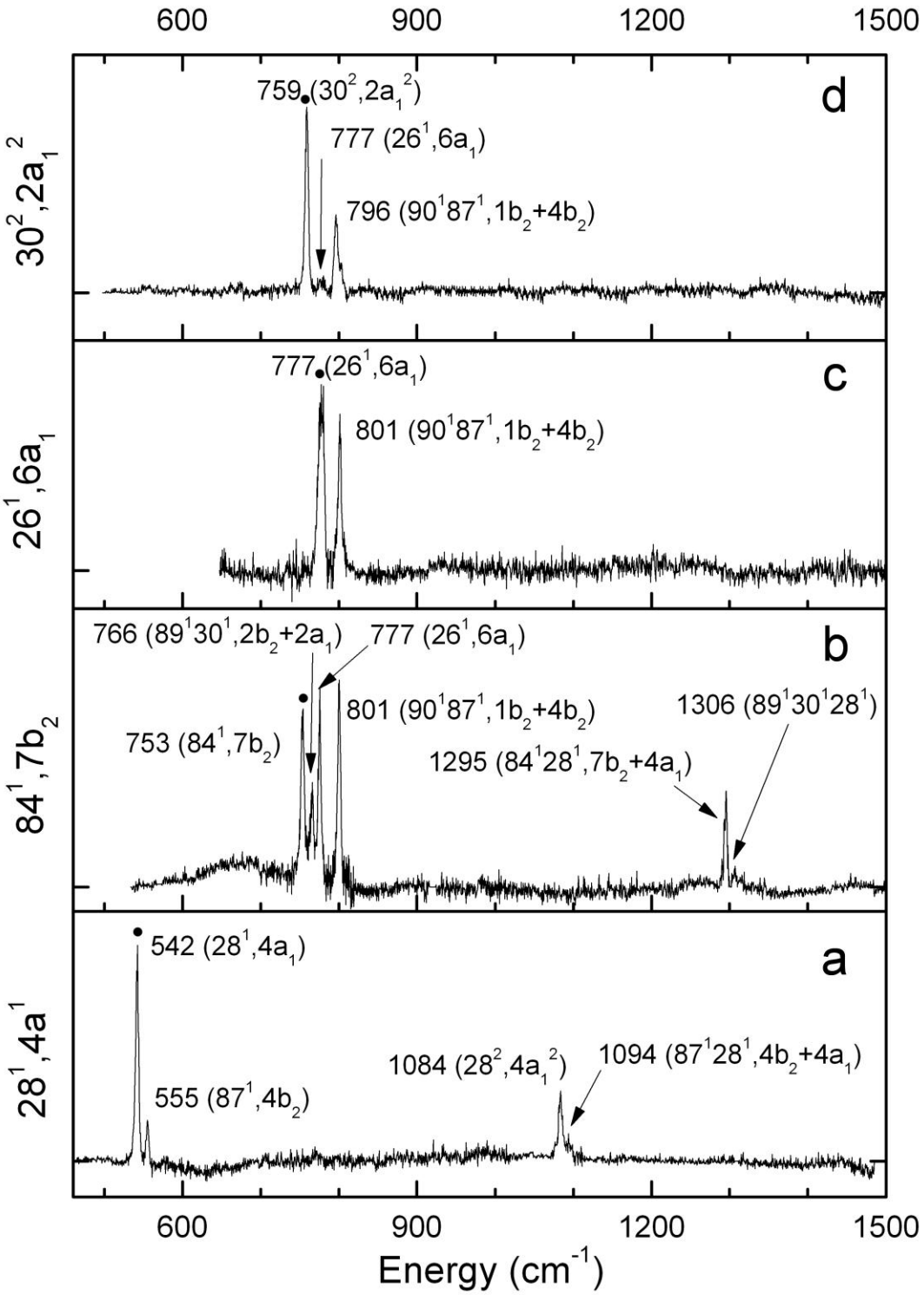
600
900
1200
1500
d
759 (30^2,2a_1^2)
777 (26^1,6a_1)
796 (90^187^1,1b_2+4b_2)
30^2,2a_1^2
c
777 (26^1,6a_1)
801 (90^187^1,1b_2+4b_2)
26^1,6a_1
b
766 (89^130^1,2b_2+2a_1)
777 (26^1,6a_1)
801 (90^187^1,1b_2+4b_2)
753 (84^1,7b_2)
1306 (89^130^128^1)
1295 (84^128^1,7b_2+4a_1)
84^1,7b_2
a
542 (28^1,4a_1)
1084 (28^2,4a_1^2)
1094 (87^128^1,4b_2+4a_1)
555 (87^1,4b_2)
28^1,4a^1
600
900
1200
1500
Energy (cm^-1)

Fig. 4

Table I Observed and calculated vibrational frequencies of the S_1 state of benzo[*e*]pyrene.

Experimental	Calculation*	Assignment	Symmetry
251	245	90^1	$1b_2$
374	377	30^1	$2a_1$
401	402	89^1	$2b_2$
537	533	28^1	$4a_1$
746	748	84^1	$7b_2$
753	753	26^1	$6a_1$
755	754	30^2	$2a_1^2$
917	929	83^1	$8b_2$
1200	1199	78^1	$13b_2$
1282	1266	76^1	$15b_2$
1312	1305	16^1	$16a_1$
1321	1317	15^1	$17a_1$
1378	1386	73^1	$18b_2$
1415	1397	13^1	$19a_1$
1478	1480	70^1	$21b_2$
1571	1586	7^1	$25a_1$

*The calculation result includes a scaling factor of 0.973.

Table II Observed and calculated vibrational frequencies of B*e*P cation.

0	90^1	30^1	89^1	28^1	84^1	26^1	30^2	Calc*	Assignment
0								0	0
	248							247	90^1 ($1b_2$)
		379						379	30^1 ($2a_1$)
			394					394	89^1 ($2b_2$)
				542				544	28^1 ($4a_1$)
				555				558	87^1 ($4b_2$)
					753			753	84^1 ($7b_2$)
							759	753	30^2 ($2a_1^2$)
					766			768	$89^1 30^1$ ($2b_2+2a_1$)
					775	***777***		771	26^1 ($6a_1$)
					801	801	796	801	$90^1 87^1$ ($1b_2+4b_2$)
				1084				1083	28^2 ($4a_1^2$)
				1094				1098	$87^1 28^1$ ($4b_2+4a_1$)
					1295			1297	$84^1 28^1$ ($7b_2+4a_1$)
					1306			1307	$89^1 30^1 28^1$

*The calculation result includes a scaling factor of 0.9697.

References

[1] L. E. Smith, M. F. Denissenko, W. P. Bennett, H. Li, S. Amin, M. S. Tang, G. P. Pfeifer, J. Natl. Cancer Inst. 92 (2000) 803.

[2] E. Kriek, M. Rojas, K. Alexandrov, H. Bartsch, Mutat. Res. Fundam. Mol. Mech. Mugag. 400 (1998) 215.

[3] R. G. Harvey, Polycyclic Aromatic Hydrocarbons: Chemistry and Carcinogenicity, Cambridge University Press, London, 1991.

[4] M. P. Bernstein, J. P. Dworkin, S. A. Sandford, G. W. Cooper, L. J. Allamandola, Nature 416 (2002) 401.

[5] S. G. Wakeham, C. Schaffner, W. Giger, Geochim. Cosmochim. 44 (1980) 415.

[6] E. L. Shock, M. D. Schulte, Nature 343 (1990) 728.

[7] P. Bréchignac, T. Pino, N. Boudin, Spectrochim. Acta, Part A 57 (2001) 745.

[8] F. Salama, G. A. Galazutdinov, J. Krelowski, L. J. Allamandola, F. A. Musaev, Astrophys. J. 526 (1999) 265.

[9] L. J. Allamandola, A. G. Tielens, J. R. Barker, Astrophys. J. 290 (1985) 125.

[10] A. Léger, J. L. Puget, Astron. Astrophys. 137 (1984).

[11] G. Malloci, G. Mulas, P. Benvenuti, Astron. Astrophys. 410 (2003) 623.

[12] G. Mulas, G. Malloci, P. Benvenuti, Astron. Astrophys. 410 (2003) 639.

[13] E. Peeters, L. J. Allamandola, D. M. Hudgins, S. Hony, A. G. G. M. Tielens, Astron. Soc. Pac. Conf. Ser. 309 (2004) 141.

[14] A. Li, PAHs in comets: An overview. In Deep Impact As a World Observatory Event: Synergies in Space, Time, and Wavelength, Springler, Berlin, 2009.

[15] Y. M. Rhee, T. J. Lee, M. S. Gudipati, L. J. Allamandola, M. Head-Gordon, Proc. Natl.

Acad. Sci. U. S. A. 104 (2007) 5274.

[16] A. Li, J. I. Lunine, Astrophys. J. 594 (2003) 987.

[17] D. M. Hudgins, L. J. Allamandola, J. Phys. Chem. 99 (1994) 3033.

[18] D. M. Hudgins, L. J. Allamandola, J. Phys. Chem. 99 (1995) 3033.

[19] D. M. Hudgins, L. J. Allamandola, J. Phys. Chem. 99 (1995) 8978.

[20] D. M. Hudgins, L. J. Allamandola, J. Phys. Chem. A 101 (1997) 3472.

[21] D. M. Hudgins, S. A. Sandford, J. Phys. Chem. A 102 (1998) 344.

[22] D. M. Hudgins, S. A. Sandford, J. Phys. Chem. A 102 (1998) 353.

[23] D. M. Hudgins, S. A. Sandford, J. Phys. Chem. A 102 (1998) 344.

[24] D. M. Hudgins, S. A. Sandford, J. Phys. Chem. A 102 (1998) 329.

[25] J. Oomens, A. J. A. Van Roij, G. Meijer, G. von Helden, Astrophys. J. 542 (2000) 404.

[26] J. Szczepanski, M. Vala, Astrophys. J. 414 (1993) 645.

[27] H. S. Kim, D. R. Wagner, R. Saykally, J. Phys. Rev. Lett. 86 (2001) 5691.

[28] M. C. R. Cockett, K. Kimura, J. Chem. Phys. 100 (1994) 3429.

[29] M. Vala, J. Szczepanski, F. Pauzat, O. Parisel, D. Talbi, Y. Ellinger, J. Phys. Chem. 98 (1994) 9187.

[30] E. W. Schlag, ZEKE spectroscopy, Cambridge University Press, London, 1998.

[31] J. Zhang, F. Han, W. Kong, J. Phys. Chem. A 114 (2010) 11117.

[32] J. Zhang, L. Pei, W. Kong, J. Chem. Phys. 128 (2008) 104301.

[33] J. Zhang, F. Han, L. Pei, W. Kong, A. Li, Astrophys. J. 715 (2010) 485.

[34] J. Zhang, C. Harthcock, W. Kong, J. Phys. Chem. A 116 (2012) 1551.

[35] J. Zhang, C. Harthcock, W. Kong, J. Chem. Phys. A 116 (2012) 7016.

[36] J. Zhang, C. Harthcock, F. Han, W. Kong, J. Chem. Phys. 135 (2011) 244306.

[37] W. E. Bachmann, J. M. Chemerda, J. Am. Chem. Soc. 60 (1938) 1023.

[38] T. Imasaka, H. Fukuoka, T. Hayashi, N. Ishibashi, Anal. Chim. Acta 156 (1984) 111.

[39] G. D. Greenblatt, E. Nissani, E. Zaroura, Y. Haas, J. Phys. Chem. 91 (1987) 570.

[40] C. M. Gittins, E. A. Rohlfing, C. M. Rohlfing, J. Chem. Phys. 105 (1996) 7323.

[41] M. N. Khan, A. A. Dwayyan, Can. J. Pure Appl. Sci. 3 (2009) 833.

[42] J. Semmler, P. Yang, Crawford., Vib. Spec. 2 (1991) 189.

[43] K. Misawa, J. Matsumoto, N. Tsuji, Y. Matsuzaki, S. Hayashi, M. Fujii, Chem. Lett. 37 (2008) 1280.

[44] J. Zhang, F. Han, W. Kong, J. Chem. Phys. A 114 (2010) 11117.

[45] M. J. Frisch, et al., Gaussian 09, Revision A.1. Gaussian, I., Ed. Wallingford CT, 2009.

[46] M. Dierksen, S. Grimme, J. Chem. Phys. 120 (2004) 3544.

[47] M. Parac, S. Grimme, J. Chem. Phys. 292 (2003) 11.

[48] J. V. Goodpaster, J. F. Harrison, V. L. McGuffin, J. Chem. Phys. 102 (1998) 3372.

[49] E. Clar, W. Schmidt, Tetrahedron 35 (1977) 1027.

[50] Y. He, C. Wu, W. Kong, J. Chem. Phys. 120 (2004) 7497.

[51] Y. He, C. Wu, W. Kong, J. Chem. Phys. 121 (2004) 3533.

[52] A. Pathak, S. Rastogi, Chem. Phys. 326 (2006) 315.